journal of
thrombosis and haemostasis

MAGT1 deficiency in XMEN disease is associated with severe platelet dysfunction and impaired platelet glycoprotein N-glycosylation

Journal:	*Journal of Thrombosis and Haemostasis*
Manuscript ID	JTH-2023-00033.R1
Article Type:	Brief Report
Date Submitted by the Author:	24-Mar-2023
Complete List of Authors:	KAUSKOT, ALEXANDRE; INSERM U1176, U1176 MALLEBRANCHE, Coralie; Université d'Angers, Université de Nantes, Inserm, CNRS, CRCI2NA, SFR ICAT; CHU Angers, Pediatric immuno-hemato-oncology Unit Bruneel, Arnaud; Hopital Bichat - Claude-Bernard, Laboratoire de Biochimie; INSERM U1193, Equipe 4 : Equipe 4 : "Mécanismes cellulaires et moléculaires de l'adaptation au stress et cancérogenèse" FENAILLE, François; Université Paris-Saclay, CEA, INRAE, Département Médicaments et Technologies pour la Santé, MetaboHUB Solarz, Jean; INSERM, U1176, VIELLARD, Toscane; INSERM, U1176 Feng, Miao; INSERM, U1176 REPERANT, Christelle; INSERM, U1176 Bordet, Jean-Claude; Hospices Civils de Lyon, Laboratoire d'hématologie; Universite Claude Bernard Lyon 1, EA 4609-Hémostase et Cancer CHOLET, Sophie; Université Paris-Saclay, CEA, INRAE, Département Médicaments et Technologies pour la Santé, MetaboHUB Denis, Cécile; INSERM, Unit 1176 McCLUSKEY, Geneviève; INSERM, U1176 LATOUR, Sylvain; INSERM, Imagine Institute, Université Paris Cité, UMR 1163 - Laboratory of Lymphocyte Activation and Susceptibility to EBV MARTIN, Emmanuel; INSERM, Imagine Institute, Université Paris Cité, UMR 1163 - Laboratory of Lymphocyte Activation and Susceptibility to EBV PELLIER, Isabelle; Université d'Angers, Université de Nantes, Inserm, CNRS, CRCI2NA, SFR ICAT; CHU Angers, Pediatric immuno-hemato-oncology Unit Lasne, Dominique; Hopital universitaire Necker-Enfants malades, Hematology; UMRS-1176, Borgel, Delphine; INSERM, U1176; Hopital universitaire Necker-Enfants malades, Hematology laboratory KRACKER, Sven; Imagine Institute, INSERM, Université Paris Cité, Laboratory of Human Lymphohematopoiesis - UMR1163 ZIEGLER, Alban C.; CHU Angers, Department of Genetics Tuffigo, Marie; CHU d'Angers, Laboratory of Hematology FOURNIER, Benjamin; Imagine Institute, INSERM, Université Paris Cité, Laboratory of Human Lymphohematopoiesis - UMR1163; Hôpital Necker

	Enfants Malades Assistance Publique-Hôpitaux de Paris, Pediatric Hematology-Immunology-Rheumatology Unit MIOT, Charline; Université d'Angers, Université de Nantes, Inserm, CNRS, CRCI2NA, SFR ICAT; CHU Angers, Pediatric immuno-hemato-oncology Unit; CHU Angers, Laboratory of Immunology and Allergology ADAM, Frédéric; INSERM, U1176
Key Words:	Congenital disorder of glycosylation, Magnesium transporter 1, N-glycosylation defect, Platelet function, XMEN disease

MAGT1 deficiency in XMEN disease is associated with severe platelet dysfunction and impaired platelet glycoprotein N-glycosylation

Alexandre Kauskot[1 &], Coralie Mallebranche[2,3 &], Arnaud Bruneel[4], François Fenaille[5], Jean Solarz[1], Toscane Viellard[1], Miao Feng[1], Christelle Repérant[1], Jean-Claude Bordet[6], Sophie Cholet[5], Cécile V. Denis[1], Geneviève McCluskey[1], Sylvain Latour[7], Emmanuel Martin[7], Isabelle Pellier[2,3], Dominique Lasne[1,8], Delphine Borgel[1,8], Sven Kracker[9], Alban Ziegler[10], Marie Tuffigo[11], Benjamin Fournier[7,12], Charline Miot[2,3,13 &&], Frédéric Adam[1 &&]

[1] INSERM U1176, Hemostasis, Inflammation & Thrombosis (HITh), Université Paris-Saclay, Le Kremlin-Bicêtre, France

[2] Université d'Angers, Université de Nantes, Inserm, CNRS, CRCI2NA, SFR ICAT, Angers, France

[3] CHU Angers, Pediatric immuno-hemato-oncology Unit, France

[4] AP-HP, Biochimie Métabolique et Cellulaire, Hôpital Bichat-Claude Bernard, Paris, France; Université Paris-Saclay, INSERM UMR1193, Mécanismes cellulaires et moléculaires de l'adaptation au stress et cancérogenèse, Châtenay-Malabry, France

[5] Université Paris-Saclay, CEA, INRAE, Département Médicaments et Technologies pour la Santé, MetaboHUB, Gif sur Yvette, France

[6] Laboratoire d'Hémostase, Centre de Biologie Est, Hospices Civils de Lyon, Bron, France

[7] Laboratory of Lymphocyte Activation and Susceptibility to EBV, INSERM UMR 1163, Imagine Institute, Université Paris Cité, Paris, France

[8] Laboratoire d'Hématologie, AP-HP, Hôpital Necker-Enfants malades, Paris, France

[9] Université Paris Cité, Laboratory of Human Lymphohematopoiesis, Imagine Institute, INSERM UMR1163, Paris, France

[10] CHU Angers, Department of Genetics, Angers, France

[11] CHU Angers, Laboratory of Hematology, Angers, France

[12] Hôpital Necker Enfants Malades Assistance Publique-Hôpitaux de Paris, Pediatric Hematology-Immunology-Rheumatology Unit, Paris, France

[13] CHU Angers, Laboratory of Immunology and Allergology, Angers, France

[&] Dr Alexandre Kauskot and Dr Coralie Mallebranche contributed equally to this work

[&&] Dr Charline Miot et Dr Frédéric Adam share senior authorship

Running head: MAGT1 deficiency and platelet dysfunction

Corresponding author: Frédéric Adam, Ph.D ; INSERM UMR_S 1176, HITh ; 80 rue du Général Leclerc, 94276 Le Kremlin-Bicêtre, France E-mail: frederic.adam@inserm.fr Tel: +33 149595650

Word count: 2199 **Abstract**: 217 **Figures:** 4 **References:** 29

ESSENTIALS

- XMEN disease is caused by loss-of-function mutations in the magnesium transporter 1 gene.
- Platelet function and N-glycosylation of platelet receptors were studied in two XMEN patients.
- Platelet dysfunction and defective N-glycosylation of platelet proteins were observed.
- These defects could explain the hemorrhages reported in XMEN patients.

ABSTRACT

Background: X-Linked immunodeficiency with magnesium defect, Epstein-Barr virus infection and neoplasia (XMEN) disease is a primary immunodeficiency due to loss-of-function mutations in the gene encoding for the magnesium transporter 1 (*MAGT1*). Furthermore, as MAGT1 is involved in the N-glycosylation process, XMEN disease is classified as a Congenital Disorder of Glycosylation. Although XMEN-associated immunodeficiency is well described, the mechanisms underlying platelet dysfunction and responsible for life-threatening bleeding events have never been investigated.

Objectives: To assess platelet functions in XMEN patients.

Patients/Methods: Two unrelated young boys, including one before and after hematopoietic stem-cell transplantation (HSCT), were investigated for their platelet functions, glycoprotein expression, and serum and platelet-derived N-glycans.

Results: Platelet analysis highlighted abnormal elongated cells and unusual barbell-shaped proplatelets. Platelet aggregation, integrin $\alpha_{IIb}\beta_3$ activation, calcium mobilization and protein kinase C (PKC) activity were impaired in both patients. Strikingly, platelet responses to protease-activated receptor 1 activating peptide (PAR1-AP) were absent at both low and high concentrations, due to the deglycosylation of PAR1. These defects were also associated with decreased molecular weight of glycoprotein (GP)Ibα, GPVI and integrin α_{IIb} due to a partial impairment of N-glycosylation. All these defects were corrected after HSCT.

Conclusions: Our results highlight prominent platelet dysfunction related to MAGT1 deficiency and a defective N-glycosylation in several platelet proteins, that could explain the hemorrhages reported in XMEN patients.

KEYWORDS

- Congenital disorder of glycosylation (CDG)
- Magnesium transporter 1 (MAGT1)
- N-glycosylation defect
- Platelet function
- XMEN disease

INTRODUCTION

X-Linked immunodeficiency with magnesium defect, Epstein-Barr virus (EBV) infection and neoplasia, called XMEN disease is a rare immunodeficiency disorder caused by loss-of-function (LOF) mutations in the magnesium transporter 1 (*MAGT1*) gene.[1-3] MAGT1 is a Mg^{2+}-specific ion transport system, involved in magnesium homeostasis in lymphocytes.[1,2] MAGT1 has also been described as a subunit in the oligosaccharyltransferase (OST) complex that transfers N-glycans onto proteins. Consequently, mutations in the *MAGT1* gene lead to Congenital Disorders of Glycosylation (CDG, MAGT1-CDG).[4] Protracted bleeding after minor surgical procedures and life-threatening bleeding events, such as intracranial hemorrhage or severe epistaxis leading to hemorrhagic shock, have been reported in XMEN patients with mild thrombocytopenia or during hematopoietic stem-cell transplantation (HSCT) procedure.[3,5] Despite the link between defective glycosylation and XMEN disease having been described,[6] no studies have investigated XMEN disease-associated platelet dysfunction. Platelet hemostatic function is regulated by glycoprotein (GP) receptors such as GPIb-IX-V complex and GPVI, integrins such as $\alpha_{IIb}\beta_3$, and G-protein-coupled receptors such as thrombin receptors termed protease-activated receptors (PARs). The function of these receptors are regulated in part by N-glycosylation,[7] however molecular mechanisms involved are poorly defined and studied in CDG.[7]

Here, we report two unrelated XMEN patients with mild bleeding events associated with platelet dysfunction and abnormal N-glycosylation of several platelet receptors.

MATERIALS AND METHODS

Patients

Two male patients were enrolled after written informed consent. Ethical approval was obtained from the local independent ethic committee (Ile-de-France II, Paris, France; CPP: 2015-01-05) and the French Advisory Committee on Data Processing in Medical Research (15.297bis). Blood samples were provided in accordance with the Declaration of Helsinki.

Preparation of washed platelets

Venous blood from healthy donors or patients was collected in 10% anticoagulant citrate dextrose solution and platelets were washed before resuspension in Tyrode's buffer, as previously described.[8]

Flow cytometry

Integrin $\alpha_{IIb}\beta_3$ activation and calcium mobilization were evaluated by flow cytometry. More details are provided in the legend of Fig. 2A,B.

Western blotting

MAGT1 expression, PKC activity and platelet receptors were investigated by western-blotting as described in the legends of Fig. 1B, 2C-D, 3. In Figures 2D and 3, washed platelets (3×10^8/mL) were lysed (1% TritonX-100, 5mM Tris-HCl, 125mM NaCl, 10mM NaF, 1x protease inhibitor cocktail), and

centrifuged at 14000 g for 20 minutes at 4°C. Supernatants were incubated for 10 minutes at 100°C with glycoprotein denaturing buffer, and treated 18 hours at 37°C with PNGaseF (25000U/mL, New England Biolabs).

Transmission electron microscopy

Platelet ultrastructure was analyzed by transmission electron microscopy.[9,10] More details are provided in the legend of Fig. 1C.

Platelet aggregation

Aggregation of washed platelets (300µL at $3x10^8$/mL) triggered by bovine thrombin, adenosine 5'-diphosphate (ADP) (Sigma), collagen (CHRONO-PAR®), or PAR1- and PAR4-activating peptides (PAR1-AP and PAR4-AP; Bachem) was monitored using a Chrono-Log Aggregometer.[11]

Analysis of transferrin glycoforms

Capillary electrophoresis transferrin profiling was performed using capillary 2 flex piercing.[12,13] More details are provided in the legend of Fig.4.

Mass spectrometry-based profiling of serum and platelet N-glycans

Analysis of serum and washed platelets N-glycans by matrix-assisted laser desorption/ionization time-of-flight mass spectrometry (MALDI-TOF MS) was performed using 2,5-dihydroxybenzoic acid solution (10mg/mL in 50% methanol containing 10mM sodium acetate) as a matrix, as previously described.[14,15] Manual assignment of N-glycans was deduced from MS and MS/MS data based on previously identified structures[15] and the GlycoWorkBench software.[16] More details are provided in the legend of Fig.4.

Statistical analysis

Data were analyzed by one-way ANOVA followed by a post-hoc test, as indicated in the figure legends. Differences were considered significant when $p<0.05$.

RESULTS AND DISCUSSION

Patients' clinical features

Patient P1 is a 7-year-old boy and second-born child to non-consanguineous Caucasian French parents. He was first referred to our center when he was 14 months for recurrent and severe infections such as several bronchiolitis, ethmoiditis, pyelonephritis and profuse varicella episodes with numerous disabling mucocutaneous lesions but without organ damage (such as brain or chest involvement). During his follow-up, he experienced a benign but delayed bleeding after a tooth extraction, several epistaxis requiring repeated cauterization and a severe hemorrhage during a testicular tissue biopsy for

fertility preservation, despite normal platelet count. Immunological tests performed at 15 months revealed low immunoglobulin levels and absence of vaccine immunization even after receiving vaccine boosts. Lymphocyte counts highlighted a persistent and prominent increased B cells count. Whole exome sequencing (WES) revealed an X-linked hemizygous missense variant in exon 8 of *MAGT1* (NM_032121.5:c.991 C>T; p.Arg331Ter, Fig. 1A) transmitted by the mother.

He was healthy under immunoglobulin replacement until he was infected by EBV at 5 years of age. Because of a high EBV viral load, he eventually underwent anti-CD20 antibody treatment followed by HSCT at the age of 7.5 years (matched sibling donor). Twelve months later, he was healthy and had not developed graft-versus-host disease.

Patient P2 is a 9-year-old boy and first-born child to non-consanguineous Caucasian French parents. P2 was followed-up at our hospital for failure to thrive due to a profound growth hormone deficiency. He had recurrent ear-nose-tract infections during early childhood, experienced a profuse varicella at 21 months and a zoster recurrence at 3 years of age. Clinical examination revealed an extensive molluscum contagiosum infection with more than 50 skin lesions. Immunological tests highlighted slightly decreased immunoglobulin levels and absence of vaccine immunization despite receiving vaccine boosts. T, B and NK cell counts were normal. Lymphocyte proliferation was normal in response to mitogens, impaired in response to tetanus toxoid, and abolished in response to varicella-zoster virus antigens. WES revealed an X-linked hemizygous insertion in exon 6 of *MAGT1* (NM_032121.5:c.786_787insCATAC; p.Thr263HisfsTer11, Fig. 1A) transmitted by the mother.

He is currently healthy under immunoglobulin replacement, growth hormone therapy and hydrocortisone supplementation.

The Combined Annotation Dependent Depletion (CADD), which is a tool for scoring the deleteriousness of single nucleotide variants, has a high score for both variants: 38 for the p.Arg331Ter and 33 for the p.Thr263HisfsTer11, suggesting nonsense-mediated decay. The p.Arg331Ter variant is classified as pathogenic in Clinvar (VCV000625837.3) and has been reported in another unrelated XMEN patient.[4] Moreover, serum transferrin analysis of both patients indicated an abnormal glycosylation pattern (Fig. 4A) with an increase in the disialylated glycoform. This suggested the presence of unoccupied N-glycosylation sites.

Thus, considering all clinical features, the predicted pathogenicity of *MAGT1* variants and the biochemical abnormalities, these patients were diagnosed with MAGT1-CDG.

XMEN patients display impaired platelet function

Platelet expression of MAGT1, which is of 2050 copies,[17] was undetectable in P1 and P2 (Fig. 1B). Absence of MAGT1 from fibroblasts and lymphocytes has previously been described in patients carrying other *MAGT1* mutations,[4] characterized as LOF variants. Analysis of hematological parameters showed normal platelet count and normal expression of key platelet receptors such as integrin $\alpha_{IIb}\beta_3$, GPIbα, GPIX, or GPVI (not shown). Platelet ultrastructure analysis demonstrated

abnormal elongated shapes in patient samples, in contrast to the discoid shaped ones of healthy donors (HDs). The unusual barbell-shaped proplatelets observed (8.2% and 8.8% for P1 and P2, respectively, *versus* 1.4% in HDs) suggested the presence of immature platelets (Fig. 1C),[18] indicating a role of MAGT1 in proplatelet maturation (further studies required). These unusual morphologies and MAGT1 expression were corrected after HSCT in P1 (Fig. 1B,C).

We next investigated the impact of the LOF of MAGT1 on platelet function in both patients. Platelet aggregation induced by low thrombin doses was impaired, but partially restored at higher concentrations (Fig. 1D). Strikingly, platelet aggregation in response to PAR1-AP was absent at low and high concentrations, and impaired at low doses of PAR4-AP (Fig. 1D). This indicated that the defects in thrombin-induced platelet aggregation were mostly dependent on PAR1 receptor. Platelet aggregation induced by collagen and ADP was also impaired (Fig. 1D). After HSCT, P1 exhibited normal aggregation profiles with all agonists tested (Fig. 1E), demonstrating that the observed defects were specifically related to MAGT1 deficiency in platelets.

To go further, activation of integrin $\alpha_{IIb}\beta_3$, a key receptor involved in platelet aggregation, was evaluated by flow cytometry (Fig. 2A). Both patients exhibited a severe deficit in integrin activation with thrombin, even at higher concentrations (56% and 71% decreases for P1 and P2 compared to HDs, respectively). Similar results were observed with convulxin and ADP. All defects were corrected in P1 after HSCT.

Integrin activation and subsequent PAR-dependent platelet aggregation, require the involvement of signaling pathways such as calcium signaling[19] and PKC activity.[20] The rapid and transient Ca^{2+} mobilization observed in HD was almost abolished in patients at low thrombin concentrations, partially impaired at higher concentrations, and corrected in P1 after HSCT (Fig. 2B). This impaired Ca^{2+} signaling could be due to a defective PAR1, to impaired magnesium homeostasis[1] and/or to functional defects in calcium channels due to abnormal N-glycosylation.[21,22] Furthermore, PKC activity was defective in P1 platelets with thrombin and PAR4-AP. No PKC activity was detected after PAR1-AP stimulation (Fig. 2C).

Due to the severe PAR1-dependent defects, PAR1 expression was investigated by western-blotting (Fig. 2D). While fully glycosylated PAR1 was detected between ~65 and ~85 kDa in HD platelets,[23] only smeared bands were observed between ~50 and ~60 kDa in P1 and P2. This result suggested a partial glycosylation defect of the receptor in patients, as incubation of platelet lysates with PNGaseF (removes all N-linked oligosaccharides from glycoproteins), eliminated the smeared bands. This partial deglycosylation could explain the PAR1-dependent defects. Indeed, it has been shown that N-glycosylation of PAR1 influences ligand docking and its signaling pathways.[24] Unfortunately, we were not able to identify fully deglycosylated PAR1. Therefore we cannot conclude whether PAR1-dependent defects were only due to the deglycosylation of PAR1, or whether they were also associated with impaired PAR1 expression.

Altogether, these results underline the severe impact of *MAGT1* mutations on PAR1-dependent platelet function, likely due to N-glycosylation defects.

Impaired platelet function in XMEN patients is associated with defective N-linked glycosylation

To further elucidate how MAGT1 deficiency could impact platelet function, we focused our investigations on defective N-linked glycosylation reported in XMEN disease.[4] We concentrated on several main platelet receptors. Integrin α_{IIb}, GPVI and GPIbα were fully glycosylated in HD samples however had lower molecular weights (MW) in XMEN samples, likely corresponding to underglycosylation (Fig. 3). To demonstrate that this decrease in MW was due to partial glycosylation of the receptors, platelet lysates were incubated with PNGaseF. A marked MW decrease of integrin α_{IIb} and GPVI by 14 kDa and 5.5 kDa, respectively, in HDs and patient samples was observed after PNGaseF treatment (Fig. 3A, B). The corresponding N-deglycosylated integrin α_{IIb} and GPVI showed no significant difference in MW between HDs and patients. These observations confirmed that the decreased MW of integrin α_{IIb} and GPVI in untreated platelets of P1 and P2 were due to a partial decrease of N-glycosylation on both receptors. Interestingly, the MW decrease did not affect all receptors in the same way; integrin β_3 and β_1 seemed normal (Fig. 3C,D) although 3 and 12 sites of N-glycosylation are predicted by NetNGlyc-1.0 server, respectively.[25] For GPIbα (Fig. 3E), a significantly lower MW band ($p<0.001$) was observed in both patients after PNGaseF treatment (130kDa) compared to HD (140kDa). This MW difference could not be attributed to an absence of sialic acid content on GPIbα, since α2-3 neuraminidase treatment did not affect it (not shown). We hypothesized that this could be due to a defect in plethoric O-glycans on GPIbα.[26] Indeed, defective N-linked glycosylation of enzymes/proteins important for O-linked glycosylation of GPIbα could cause this MW shift. This was also suggested for the defect observed in XMEN on apolipoprotein-CIII, which carries an O-glycosylation site.[6] Unfortunately, we were not able to confirm this hypothesis as O-glycosidase treatment of patient platelets prevented any correct detection of proteins by western blotting. Finally, in P1, all receptors analyzed recovered normal MW after HSCT, indicating an intrinsic role of MAGT1 in platelets.

Altogether, these data demonstrate a partial N-linked glycosylation defect on glycoproteins in platelets as previously described for the NKG2D receptor in T lymphocytes.[6]

To further characterize the XMEN-associated glycosylation defects, we analyzed N-glycosylation of liver-derived serum transferrin, and total serum and platelet N-glycomes from patients. Transferrin N-glycosylation patterns in patients showed a decrease in the major tetrasialylated glycoform compared to HDs, and a distinctive increase in the disialylated glycoform (Fig. 4A). N-glycoprotein macroheterogeneity arises from variations in N-glycosylation site occupancy, while microheterogeneity concerns the variations of N-glycan structures at a specific N-glycosylation site. Macroheterogeneity is caused by inefficient transfer of N-glycans to proteins, which is determined by the presence and function of OST subunits. Similar to how the OST complex is impacted in Signal Sequence Receptor Subunit 4 (SSR4)-CDG,[27] this result suggests the loss of one of two N-glycan chains of transferrin, therefore a partial under-occupancy of its glycosylation sites (macroheterogeneity). However total

serum and platelet N-glycan profiles of the patients proved overall similar to HD regarding N-glycan structures and corresponding relative abundancies, demonstrating absence of microheterogeneity (Fig. 4B,C). Therefore, these results consistently underline that XMEN patients can present partial (in the liver) or total (in platelets) defective N-glycosylation macroheterogeneity (for some proteins), without impacting N-glycan microheterogeneity. Hence, we hypothesize that the decreased MW of platelet receptors (Fig. 3) could be due to a partial defect of N-glycosylation site occupancy without modifications to the N-glycan structures.

In conclusion, we described here for the first time in two unrelated XMEN patients that MAGT1 deficiency has significant negative impacts on platelet function, causing severe thrombopathy, possibly by altering N-glycosylation in several platelet proteins.

ACKNOWLEDGMENTS

We are grateful to patients and their families for their cooperation in the study. We thank the CIQLE Centre d'Imagerie Quantitative Lyon-Est (France) for expert technical assistance with the electron microscopy studies and CEDI (Centre d'Etude des Déficits Immunitaires; Hôpital Necker-Enfants Malades, Paris, France) for biological investigations. This work was supported by INSERM.

AUTHOR CONTRIBUTIONS

AK, JS, MF, TV, CR, JCB, AB, FF, SC, DL, SK, AZ, FA designed, performed experiments, collected and analyzed the data; AK, CR, CM, FA wrote the manuscript; DB, CD, GMC, SL, EM critically reviewed the manuscript; CM, MT, BF, IP provided patient and family care, and monitored the patients.

CONFLICT OF INTEREST

The authors declare no conflict of interest.

REFERENCES

1. Li FY, Chaigne-Delalande B, Kanellopoulou C, et al. Second messenger role for Mg2+ revealed by human T-cell immunodeficiency. *Nature*. 2011;475(7357):471-476.

2. Chaigne-Delalande B, Li FY, O'Connor GM, et al. Mg2+ regulates cytotoxic functions of NK and CD8 T cells in chronic EBV infection through NKG2D. *Science*. 2013;341(6142):186-191.

3. Li FY, Chaigne-Delalande B, Su H, Uzel G, Matthews H, Lenardo MJ. XMEN disease: a new primary immunodeficiency affecting Mg2+ regulation of immunity against Epstein-Barr virus. *Blood*. 2014;123(14):2148-2152.

4. Blommaert E, Peanne R, Cherepanova NA, et al. Mutations in MAGT1 lead to a glycosylation disorder with a variable phenotype. *Proceedings of the National Academy of Sciences of the United States of America*. 2019;116(20):9865-9870.

5. Dimitrova D, Rose JJ, Uzel G, et al. Successful Bone Marrow Transplantation for XMEN: Hemorrhagic Risk Uncovered. *Journal of clinical immunology*. 2019;39(1):1-3.

6. Ravell JC, Matsuda-Lennikov M, Chauvin SD, et al. Defective glycosylation and multisystem abnormalities characterize the primary immunodeficiency XMEN disease. *The Journal of clinical investigation*. 2020;130(1):507-522.

7. Mammadova-Bach E, Jaeken J, Gudermann T, Braun A. Platelets and Defective N-Glycosylation. *International journal of molecular sciences*. 2020;21(16).

8. Adam F, Verbeuren TJ, Fauchere JL, Guillin MC, Jandrot-Perrus M. Thrombin-induced platelet PAR4 activation: role of glycoprotein Ib and ADP. *Journal of thrombosis and haemostasis : JTH*. 2003;1(4):798-804.

9. Berrou E, Soukaseum C, Favier R, et al. A mutation of the human EPHB2 gene leads to a major platelet functional defect. *Blood*. 2018;132(19):2067-2077.

10. Nurden P, Chretien F, Poujol C, Winckler J, Borel-Derlon A, Nurden A. Platelet ultrastructural abnormalities in three patients with type 2B von Willebrand disease. *British journal of haematology*. 2000;110(3):704-714.

11. Adam F, Kauskot A, Nurden P, et al. Platelet JNK1 is involved in secretion and thrombus formation. *Blood*. 2010;115(20):4083-4092.

12. Jeppsson JO, Arndt T, Schellenberg F, et al. Toward standardization of carbohydrate-deficient transferrin (CDT) measurements: I. Analyte definition and proposal of a candidate reference method. *Clinical chemistry and laboratory medicine*. 2007;45(4):558-562.

13. Parente F, Ah Mew N, Jaeken J, Gilfix BM. A new capillary zone electrophoresis method for the screening of congenital disorders of glycosylation (CDG). *Clinica chimica acta; international journal of clinical chemistry*. 2010;411(1-2):64-66.

14. Bruneel A, Cholet S, Drouin-Garraud V, et al. Complementarity of electrophoretic, mass spectrometric, and gene sequencing techniques for the diagnosis and characterization of congenital disorders of glycosylation. *Electrophoresis*. 2018;39(24):3123-3132.

15. Goyallon A, Cholet S, Chapelle M, Junot C, Fenaille F. Evaluation of a combined glycomics and glycoproteomics approach for studying the major glycoproteins present in biofluids: Application to cerebrospinal fluid. *Rapid communications in mass spectrometry : RCM*. 2015;29(6):461-473.

16. Ceroni A, Maass K, Geyer H, Geyer R, Dell A, Haslam SM. GlycoWorkbench: a tool for the computer-assisted annotation of mass spectra of glycans. *Journal of proteome research*. 2008;7(4):1650-1659.

17. Huang J, Swieringa F, Solari FA, et al. Assessment of a complete and classified platelet proteome from genome-wide transcripts of human platelets and megakaryocytes covering platelet functions. *Scientific reports*. 2021;11(1):12358.

18. Kemble S, Dalby A, Lowe GC, et al. Analysis of preplatelets and their barbell platelet derivatives by imaging flow cytometry. *Blood advances*. 2022;6(9):2932-2946.

19. Varga-Szabo D, Braun A, Nieswandt B. Calcium signaling in platelets. *Journal of thrombosis and haemostasis : JTH*. 2009;7(7):1057-1066.

20. Harper MT, Poole AW. Diverse functions of protein kinase C isoforms in platelet activation and thrombus formation. *Journal of thrombosis and haemostasis : JTH*. 2010;8(3):454-462.

21. Choi YJ, Zhao Y, Bhattacharya M, Stathopulos PB. Structural perturbations induced by Asn131 and Asn171 glycosylation converge within the EFSAM core and enhance stromal interaction molecule-1 mediated store operated calcium entry. *Biochimica et biophysica acta Molecular cell research*. 2017;1864(6):1054-1063.

22. Dietrich A, Mederos y Schnitzler M, Emmel J, Kalwa H, Hofmann T, Gudermann T. N-linked protein glycosylation is a major determinant for basal TRPC3 and TRPC6 channel activity. *The Journal of biological chemistry*. 2003;278(48):47842-47852.

23. Vouret-Craviari V, Grall D, Chambard JC, Rasmussen UB, Pouyssegur J, Van Obberghen-Schilling E. Post-translational and activation-dependent modifications of the G protein-coupled thrombin receptor. *The Journal of biological chemistry*. 1995;270(14):8367-8372.

24. Soto AG, Trejo J. N-linked glycosylation of protease-activated receptor-1 second extracellular loop: a critical determinant for ligand-induced receptor activation and internalization. *The Journal of biological chemistry*. 2010;285(24):18781-18793.

25. Gupta R, Brunak S. Prediction of glycosylation across the human proteome and the correlation to protein function. *Pacific Symposium on Biocomputing Pacific Symposium on Biocomputing*. 2002:310-322.

26. Li Y, Fu J, Ling Y, et al. Sialylation on O-glycans protects platelets from clearance by liver Kupffer cells. *Proceedings of the National Academy of Sciences of the United States of America*. 2017;114(31):8360-8365.

27. Castiglioni C, Feillet F, Barnerias C, et al. Expanding the phenotype of X-linked SSR4-CDG: Connective tissue implications. *Human mutation*. 2021;42(2):142-149.

28. Feng M, Elaib Z, Borgel D, et al. NAADP/SERCA3-Dependent Ca(2+) Stores Pathway Specifically Controls Early Autocrine ADP Secretion Potentiating Platelet Activation. *Circulation research*. 2020;127(7):e166-e183.

29. Watanabe Y, Aoki-Kinoshita KF, Ishihama Y, Okuda S. GlycoPOST realizes FAIR principles for glycomics mass spectrometry data. *Nucleic acids research*. 2021;49(D1):D1523-D1528.

FIGURE LEGENDS

Figure 1. Severe platelet dysfunction due to MAGT1 deficiency in XMEN disease

(**A**) Schematic representation of MAGT1 protein and localization of the two mutations carried by XMEN patients (P1 and P2). MAGT1 consists of a signal peptide (SP), a thioredoxin domain and four transmembrane (TM) regions.

(**B**) MAGT1 expression was evaluated in platelets of healthy donors (HDs) or XMEN patients by western-blotting. For P1, MAGT1 expression was also assessed after HSCT. Washed platelets ($3x10^8$/mL) were lysed in Laemmli sample buffer and reduced with 25 mM dithiothreitol (DTT). Platelet lysates (corresponding to $5x10^6$ platelets) were loaded onto the gel, separated by electrophoresis using a NuPage™ 4-12% Bis-Tris Protein gel (Invitrogen), then transferred to nitrocellulose membrane. Membranes were incubated overnight with the primary antibodies rabbit anti-MAGT1 (0.2 µg/mL; Proteintech) or mouse anti-β-actin (1/10000, used as loading control; R&D Systems), then with the secondary horseradish peroxidase (HRP)-coupled antibodies (Interchim): donkey anti-mouse IgG-HRP (1/10000, Interchim) or donkey anti-rabbit IgG-HRP (1/10000). Immunoreactive bands were visualized with enhanced chemiluminescence detection reagents (ECL) using a G:BOX Chemi XT16 Image System, then quantified using Gene Tools version 4.03.05.0 (Syngene). Representative blot (left panel) and mean ± SEM of MAGT1 expression (right graph) normalized to β-actin (HD is set to 1) from several independent experiments (HDs, *n* = 9; P1, *n* = 3; P1 after HSCT, *n* = 5; P2, *n* = 3) are presented. Statistical difference was evaluated by one-way ANOVA with Dunnett's post-test for multiple comparisons (*** p<0.001).

(**C**) Platelet ultrastructure was analyzed once for each patient using transmission electron microscopy (TEM). Platelet-rich plasma (PRP) was fixed by incubating for 1 hour at room temperature with 1.25% glutaraldehyde in 0.1 M phosphate buffer, pH 7.2, centrifuged for 10 minutes at 1100g, and washed once in phosphate buffer. Platelets were kept in 0.2% glutaraldehyde at 4°C until being processed by standard TEM for analysis of platelet morphology, as previously described.[9,10] Pictures represent two different magnifications (bottom higher magnification). Scale bar represents 1 µm. Graph shows the platelet morphology which is defined by the ratio between the large and the small diameter of the platelet. One hundred platelets were analyzed by TEM, and the graph represents the mean ± SEM. Statistical difference was evaluated by one-way ANOVA with Dunnett's post-test for multiple comparisons (* p<0.05).

(**D,E**) Aggregation of washed platelets (300 µL at 3.10^8/mL) induced by thrombin (80 and 150 mU/mL), PAR1-AP (10 and 100 µM), PAR4-AP (50 and 100 µM), collagen (1 and 2 µg/mL) or ADP (10 and 50 µM) was evaluated once for each patient (P1, P2 and P1 after HSCT) and HD.

Figure 2. Impairment of integrin $\alpha_{IIb}\beta_3$ activation, calcium signaling, PKC activity and glycosylated PAR1 due to MAGT1 deficiency in XMEN disease

(**A**) Integrin $\alpha_{IIb}\beta_3$ activation was evaluated once for each patient by flow cytometry (BD AccuriC6Plus), using a specific antibody, PAC1, which recognizes the active conformation of the integrin. Washed

platelets ($2x10^8$/mL) in Tyrode's buffer were stimulated or not for 10 minutes without stirring by a range of thrombin (100 to 1000 mU/mL), convulxin (75 to 600 pM; Pentapharm) or ADP (10 to 100 µM) concentrations. Platelet stimulation was then stopped by adding 1 mL Tyrode's buffer containing 2 mM $CaCl_2$, before incubation with fluorescein isothiocyanate (FITC) anti-human-activated $\alpha_{IIb}\beta_3$ integrin (clone PAC-1; Becton Dickinson; 20 µL of FITC-PAC1 for $5x10^5$ platelets) for 20 minutes at room temperature. Graphs represent the relative mean fluorescence intensity (MFI) of PAC1-binding to platelets of P1 (red; n=1), P2 (green; n=1) and P1 after HSCT (blue; n=1), compared to that of HD (black; n=3) platelets at the highest dose of thrombin (1000 mU/mL), convulxin (600 pM) or ADP (100 µM) that is set as 100%.

(**B**) Calcium mobilization was assessed once for HD (black), P1 (red), P2 (green) and P1 after HSCT (blue) by flow cytometry. Washed platelets ($3x10^8$/mL) were preincubated with the calcium fluorophore Oregon-green 488 BAPTA-1 AM (1 µM, Invitrogen) for 30 minutes à 37°C, then diluted at $3x10^6$/ mL in Tyrode's buffer. Calcium mobilization induced by thrombin (50 or 200 mU/mL) in absence of external Ca^{2+} (supplemented with EGTA 0.1 mM) was recorded in real time by flow cytometry as previously described.[28] The graphs represent Ca^{2+} mobilization defined as the ratio of MFI of activated *versus* resting platelets (set as 1) as a function of time in seconds. Arrow indicates the time of platelet stimulation by thrombin.

(**C**) PKC activity in HD and P1 platelets after stimulation for 3 minutes with a range of thrombin (90 to 500 mU/mL), PAR1-AP (10 to 100 µM) or PAR4-AP (75 to 100 µM) concentrations was indirectly analyzed once by assessing serine phosphorylation of PKC substrates by western-blotting. Washed platelets ($3x10^8$/mL) were lysed in Laemmli sample buffer and reduced with 25 mM DTT. Platelet lysates (corresponding to $5x10^6$ platelets) were loaded onto the gel, separated by electrophoresis using a NuPage™ 4-12% Bis-Tris Protein gel, then transferred to nitrocellulose membrane. Membranes were incubated overnight with the primary antibodies rabbit anti-Phospho-(Ser) PKC substrate (1/1000; Cell Signaling) or rabbit anti-14-3-3ζ (0.2 µg/mL; Santa Cruz), used as loading control for normalization, then with the secondary HRP-coupled antibody donkey anti-rabbit IgG-HRP (1/10000). The graphs show the phosphorylation index in arbitrary units (a.u.) obtained by the ratio between the signal intensity of a lane and that obtained without stimulation.

(**D**) PAR1 expression was evaluated in HD, P1, P2, P1 after HSCT (P1-H) and PNGase F-treated HD platelets by western-blotting. Platelet lysates ($5x10^6$ platelets) were reduced with 25 mM DTT and separated by electrophoresis using a NuPage™ 4-12% Bis-Tris Protein gel and transferred to nitrocellulose membrane. PAR1 protein was detected using mouse anti-PAR1 antibody (1 µg/mL; Clone ATAP2; Santa Cruz) and mouse anti-β-actin (1/10000) was used as loading control. In (C and D), dotted lines indicate that the samples were derived from the same gel but were non-contiguous. Arrow indicates a non-specific band because it was also found with mouse platelets (not shown), which do not express PAR1.

Figure 3. Restricted N-linked glycosylation of platelet glycoproteins

The molecular weights (MW) of (**A**) integrin α_{IIb}, (**B**) GPVI, (**C**) integrin β_3, (**D**) integrin β_1 and (**E**) GPIbα were evaluated in platelet lysates from healthy donors (HD), P1, P2 and P1 after HSCT (P1-H) by western-blotting before and after treatment with PNGase F. Washed platelets ($3x10^8$/mL) or PNGase F-treated platelets ($3x10^8$/mL) were lysed in Laemmli sample buffer and reduced with 25 mM DTT. Platelet lysates (corresponding to $5x10^6$ platelets) were loaded onto the gel, separated by electrophoresis using a NuPage™ 4-12% Bis-Tris Protein gel, then transferred to nitrocellulose membrane. Membranes were incubated overnight with the primary antibodies : mouse anti-CD41 (0.2 µg/mL, clone SZ22; Beckman Coulter), mouse anti-CD42b (GPIbα, 1 µg/mL, clone SZ2; Beckman Coulter), mouse anti-CD61 (0.05 µg/mL, clone 1; Beckman Coulter), rabbit anti-integrin β1 (0.2 µg/mL; Proteintech), or sheep anti-GPVI (0.2 µg/mL; R&D Systems), then with the secondary HRP-coupled antibodies: donkey anti-mouse IgG-HRP (1/10000), donkey anti-rabbit IgG-HRP (1/10000) or donkey anti-sheep IgG-HRP (1/5000). The graphs represent the mean MW variation ± SEM, (in kDa), for the patients compared to HDs, from at least 3 independent measures (for integrin α_{IIb} without treatment: HDs, n = 12; P1, n = 7; P1-HSCT, n = 4; P2, n = 5; for integrin α_{IIb} with PNGase F: HDs, n = 5; P1, n = 4; P1-HSCT, n = 3; P2, n = 4; for GPVI without treatment: HDs, n = 12; P1, n = 8; P1-HSCT, n = 9; P2, n = 8; for GPVI with PNGase F: HDs, n = 5; P1, n = 5; P1-HSCT, n = 9; P2, n = 8; for integrin β_3 without treatment: HDs, n = 11; P1, n = 6; P1-HSCT, n = 4; P2, n = 4; for integrin β_3 with PNGase F: HDs, n = 3; P1, n = 3; P1-HSCT, n = 3; P2, n = 3; for integrin β_1 without treatment: HDs, n = 9; P1, n = 7; P1-HSCT, n = 7; P2, n = 7; for integrin β_1 with PNGase F: HDs, n = 4; P1, n = 4; P1-HSCT, n = 4; P2, n = 4; for GPIbα without treatment: HDs, n = 17; P1, n = 11; P1-HSCT, n = 4; P2, n = 5; for GPIbα with PNGase F: HDs, n = 7; P1, n = 6; P1-HSCT, n = 4; P2, n = 4). In (**D**), arrows indicate mature integrin β_1 (#1) and N-deglycosylated integrin β_1 (#2). Statistical difference was evaluated by one-way ANOVA with Dunnett's post-test for multiple comparisons (*** $p< 0.001$).

Figure 4. N-glycosylation analysis of liver-derived serum transferrin and mass spectrometry-based profiling of serum and platelet N-glycans

(**A**) The capillary electrophoresis transferrin (Tf) profile was investigated for healthy donor (HD), P1, P1 after HSCT and P2. Briefly, Tf glycoforms were separated and further detected at 200 nm wavelength using the capillary electrophoresis CDT kit from Sebia (France), originally developed for alcohol abuse screening.[12,13] Tf glycoforms are separated based on their electrophoretic mobility, which depends on their charge and size. The number of negatively-charged terminal sialic acids affects charge, while the number and length of N-glycan chains affect the size. Using this kit in HDs, 4-sialo Tf corresponds to Tf bearing two complete biantennary, disialylated N-glycan chains; 5-sialo Tf corresponds to 4-sialo Tf bearing an additional sialylated antennae on one chain; 3-sialo Tf corresponds to 4-sialo Tf lacking one terminal sialic acid moiety; and 2-sialo Tf classically corresponds to the absence of one entire N-glycan chain (as depicted in the P1 profile). In patients, elevated 2-sialo Tf highlights the partial lack of one entire N-glycan chain in agreement with defects in the OST complex. Graphs represent, in y axis, the optical density and the migration time in arbitrary units (a.u.), in the x axis. The glycoform distributions

for HD, P1 before and after HSCT, and P2 are indicated in the table. Normal range values have been established internally after using CDT kit for several years.

(**B, C**) MALDI-TOF mass spectra of permethylated PNGase F-released N-glycans from (**B**) serum and (**C**) platelet samples. Measurements were performed in the positive-ion mode and all ions are present in sodiated [M+Na^+] form. Green circles, mannose; yellow circles, galactose; blue squares, N-acetyl glucosamine; red triangles, fucose ; purple diamonds, sialic acid. (*) polyhexose species. Briefly, serum samples (5 µL) and washed platelets ($5x10^6$) were diluted in 100 mM sodium phosphate buffer (pH 7.4) and 100 mM dithiothreitol solutions (final concentrations 20 mM and 10 mM, respectively, in a total volume of 49 µL) and glycoproteins were denatured by heating to 95°C for 5 min. Protein de-N-glycosylation consisted in incubating overnight at 37°C with 2U of PNGase F. After acidification, proteins were precipitated using ice-cold ethanol for 1 hour at -20°C. N-glycans released were purified using porous graphitic carbon solid phase extraction cartridges, and subsequently permethylated before another purification step using C18 spin-columns. MALDI-TOF mass spectra were obtained by accumulating 1000–5000 shots (depending on the samples) over the 500–5000 *m/z* range, and were further internally calibrated. Glycan calibrants used were [$Man_5HexNAc_2$ + Na^+] at *m/z* 1579.783, [$Gal_1Man_3HexNAc_2Fuc_1$ + Na^+] at *m/z* 2040.025, [$Sial_1Gal_2Man_3HexNAc_4$ + Na^+] at *m/z* 2431.209, [$Sial_2Gal_2Man_3HexNAc_4$ + Na^+] at *m/z* 2792.383, and [$Sial_3Gal_3Man_3HexNAc_5$ + Na^+] at *m/z* 3602.776. All glycomics data are available on https://glycopost.glycosmos.org[29] under the accession number GPST000333.

MAGT1 deficiency in XMEN disease is associated with severe platelet dysfunction and impaired platelet glycoprotein N-glycosylation

Alexandre Kauskot[1 &], Coralie Mallebranche[2,3 &], Arnaud Bruneel[4], François Fenaille[5], Jean Solarz[1], Toscane Viellard[1], Miao Feng[1], Christelle Repérant[1], Jean-Claude Bordet[6], Sophie Cholet[5], Cécile V. Denis[1], Geneviève McCluskey[1], Sylvain Latour[7], Emmanuel Martin[7], Isabelle Pellier[2,3], Dominique Lasne[1,8], Delphine Borgel[1,8], Sven Kracker[9], Alban Ziegler[10], Marie Tuffigo[11], Benjamin Fournier[7,12], Charline Miot[2,3,13 &&], Frédéric Adam[1 &&]

[1] INSERM U1176, Hemostasis, Inflammation & Thrombosis (HITh), Université Paris-Saclay, Le Kremlin-Bicêtre, France

[2] Université d'Angers, Université de Nantes, Inserm, CNRS, CRCI2NA, SFR ICAT, Angers, France

[3] CHU Angers, Pediatric immuno-hemato-oncology Unit, France

[4] AP-HP, Biochimie Métabolique et Cellulaire, Hôpital Bichat-Claude Bernard, Paris, France; Université Paris-Saclay, INSERM UMR1193, Mécanismes cellulaires et moléculaires de l'adaptation au stress et cancérogenèse, Châtenay-Malabry, France

[5] Université Paris-Saclay, CEA, INRAE, Département Médicaments et Technologies pour la Santé, MetaboHUB, Gif sur Yvette, France

[6] Laboratoire d'Hémostase, Centre de Biologie Est, Hospices Civils de Lyon, Bron, France

[7] Laboratory of Lymphocyte Activation and Susceptibility to EBV, INSERM UMR 1163, Imagine Institute, Université Paris Cité, Paris, France

[8] Laboratoire d'Hématologie, AP-HP, Hôpital Necker-Enfants malades, Paris, France

[9] Université Paris Cité, Laboratory of Human Lymphohematopoiesis, Imagine Institute, INSERM UMR1163, Paris, France

[10] CHU Angers, Department of Genetics, Angers, France

[11] CHU Angers, Laboratory of Hematology, Angers, France

[12] Hôpital Necker Enfants Malades Assistance Publique-Hôpitaux de Paris, Pediatric Hematology-Immunology-Rheumatology Unit, Paris, France

[13] CHU Angers, Laboratory of Immunology and Allergology, Angers, France

[&] Dr Alexandre Kauskot and Dr Coralie Mallebranche contributed equally to this work

[&&] Dr Charline Miot et Dr Frédéric Adam share senior authorship

Running head: MAGT1 deficiency and platelet dysfunction

Corresponding author: Frédéric Adam, Ph.D ; INSERM UMR_S 1176, HITh ; 80 rue du Général Leclerc, 94276 Le Kremlin-Bicêtre, France E-mail: frederic.adam@inserm.fr Tel: +33 149595650

Word count: 2199 **Abstract**: 217 **Figures:** 4 **References:** 29

ESSENTIALS

- XMEN disease is caused by loss-of-function mutations in the magnesium transporter 1 gene.
- Platelet function and N-glycosylation of platelet receptors were studied in two XMEN patients.
- Platelet dysfunction and defective N-glycosylation of platelet proteins were observed.
- These defects could explain the hemorrhages reported in XMEN patients.

ABSTRACT

Background: X-Linked immunodeficiency with magnesium defect, Epstein-Barr virus infection and neoplasia (XMEN) disease is a primary immunodeficiency due to loss-of-function mutations in the gene encoding for the magnesium transporter 1 (*MAGT1*). Furthermore, as MAGT1 is involved in the N-glycosylation process, XMEN disease is classified as a Congenital Disorder of Glycosylation. Although XMEN-associated immunodeficiency is well described, the mechanisms underlying platelet dysfunction and responsible for life-threatening bleeding events have never been investigated.

Objectives: To assess platelet functions in XMEN patients.

Patients/Methods: Two unrelated young boys, including one before and after hematopoietic stem-cell transplantation (HSCT), were investigated for their platelet functions, glycoprotein expression, and serum and platelet-derived N-glycans.

Results: Platelet analysis highlighted abnormal elongated cells and unusual barbell-shaped proplatelets. Platelet aggregation, integrin $\alpha_{IIb}\beta_3$ activation, calcium mobilization and protein kinase C (PKC) activity were impaired in both patients. Strikingly, platelet responses to protease-activated receptor 1 activating peptide (PAR1-AP) were absent at both low and high concentrations, due to the deglycosylation of PAR1. These defects were also associated with decreased molecular weight of glycoprotein (GP)Ibα, GPVI and integrin α_{IIb} due to a partial impairment of N-glycosylation. All these defects were corrected after HSCT.

Conclusions: Our results highlight prominent platelet dysfunction related to MAGT1 deficiency and a defective N-glycosylation in several platelet proteins, that could explain the hemorrhages reported in XMEN patients.

KEYWORDS

- Congenital disorder of glycosylation (CDG)
- Magnesium transporter 1 (MAGT1)
- N-glycosylation defect
- Platelet function
- XMEN disease

INTRODUCTION

X-Linked immunodeficiency with magnesium defect, Epstein-Barr virus (EBV) infection and neoplasia, called XMEN disease is a rare immunodeficiency disorder caused by loss-of-function (LOF) mutations in the magnesium transporter 1 (*MAGT1*) gene.[1-3] MAGT1 is a Mg^{2+}-specific ion transport system, involved in magnesium homeostasis in lymphocytes.[1,2] MAGT1 has also been described as a subunit in the oligosaccharyltransferase (OST) complex that transfers N-glycans onto proteins. Consequently, mutations in the *MAGT1* gene lead to Congenital Disorders of Glycosylation (CDG, MAGT1-CDG).[4] Protracted bleeding after minor surgical procedures and life-threatening bleeding events, such as intracranial hemorrhage or severe epistaxis leading to hemorrhagic shock, have been reported in XMEN patients with mild thrombocytopenia or during hematopoietic stem-cell transplantation (HSCT) procedure.[3,5] Despite the link between defective glycosylation and XMEN disease having been described,[6] no studies have investigated XMEN disease-associated platelet dysfunction. Platelet hemostatic function is regulated by glycoprotein (GP) receptors such as GPIb-IX-V complex and GPVI, integrins such as $\alpha_{IIb}\beta_3$, and G-protein-coupled receptors such as thrombin receptors termed protease-activated receptors (PARs). The function of these receptors are regulated in part by N-glycosylation,[7] however molecular mechanisms involved are poorly defined and studied in CDG.[7]

Here, we report two unrelated XMEN patients with mild bleeding events associated with platelet dysfunction and abnormal N-glycosylation of several platelet receptors.

MATERIALS AND METHODS

Patients

Two male patients were enrolled after written informed consent. Ethical approval was obtained from the local independent ethic committee (Ile-de-France II, Paris, France; CPP: 2015-01-05) and the French Advisory Committee on Data Processing in Medical Research (15.297bis). Blood samples were provided in accordance with the Declaration of Helsinki.

Preparation of washed platelets

Venous blood from healthy donors or patients was collected in 10% anticoagulant citrate dextrose solution and platelets were washed before resuspension in Tyrode's buffer, as previously described.[8]

Flow cytometry

Integrin $\alpha_{IIb}\beta_3$ activation and calcium mobilization were evaluated by flow cytometry. More details are provided in the legend of Fig. 2A,B.

Western blotting

MAGT1 expression, PKC activity and platelet receptors were investigated by western-blotting as described in the legends of Fig. 1B, 2C-D, 3. In Figures 2D and 3, washed platelets (3×10^8/mL) were lysed (1% TritonX-100, 5mM Tris-HCl, 125mM NaCl, 10mM NaF, 1x protease inhibitor cocktail), and

centrifuged at 14000 g for 20 minutes at 4°C. Supernatants were incubated for 10 minutes at 100°C with glycoprotein denaturing buffer, and treated 18 hours at 37°C with PNGaseF (25000U/mL, New England Biolabs).

Transmission electron microscopy

Platelet ultrastructure was analyzed by transmission electron microscopy.[9,10] More details are provided in the legend of Fig. 1C.

Platelet aggregation

Aggregation of washed platelets (300µL at $3x10^8$/mL) triggered by bovine thrombin, adenosine 5'-diphosphate (ADP) (Sigma), collagen (CHRONO-PAR®), or PAR1- and PAR4-activating peptides (PAR1-AP and PAR4-AP; Bachem) was monitored using a Chrono-Log Aggregometer.[11]

Analysis of transferrin glycoforms

Capillary electrophoresis transferrin profiling was performed using capillary 2 flex piercing.[12,13] More details are provided in the legend of Fig.4.

Mass spectrometry-based profiling of serum and platelet N-glycans

Analysis of serum and washed platelets N-glycans by matrix-assisted laser desorption/ionization time-of-flight mass spectrometry (MALDI-TOF MS) was performed using 2,5-dihydroxybenzoic acid solution (10mg/mL in 50% methanol containing 10mM sodium acetate) as a matrix, as previously described.[14,15] Manual assignment of N-glycans was deduced from MS and MS/MS data based on previously identified structures[15] and the GlycoWorkBench software.[16] More details are provided in the legend of Fig.4.

Statistical analysis

Data were analyzed by one-way ANOVA followed by a post-hoc test, as indicated in the figure legends. Differences were considered significant when $p<0.05$.

RESULTS AND DISCUSSION

Patients' clinical features

Patient P1 is a 7-year-old boy and second-born child to non-consanguineous Caucasian French parents. He was first referred to our center when he was 14 months for recurrent and severe infections such as several bronchiolitis, ethmoiditis, pyelonephritis and profuse varicella episodes with numerous disabling mucocutaneous lesions but without organ damage (such as brain or chest involvement). During his follow-up, he experienced a benign but delayed bleeding after a tooth extraction, several epistaxis requiring repeated cauterization and a severe hemorrhage during a testicular tissue biopsy for

fertility preservation, despite normal platelet count. Immunological tests performed at 15 months revealed low immunoglobulin levels and absence of vaccine immunization even after receiving vaccine boosts. Lymphocyte counts highlighted a persistent and prominent increased B cells count. Whole exome sequencing (WES) revealed an X-linked hemizygous missense variant in exon 8 of *MAGT1* (NM_032121.5:c.991 C>T; p.Arg331Ter, Fig. 1A) transmitted by the mother.

He was healthy under immunoglobulin replacement until he was infected by EBV at 5 years of age. Because of a high EBV viral load, he eventually underwent anti-CD20 antibody treatment followed by HSCT at the age of 7.5 years (matched sibling donor). Twelve months later, he was healthy and had not developed graft-versus-host disease.

Patient P2 is a 9-year-old boy and first-born child to non-consanguineous Caucasian French parents. P2 was followed-up at our hospital for failure to thrive due to a profound growth hormone deficiency. He had recurrent ear-nose-tract infections during early childhood, experienced a profuse varicella at 21 months and a zoster recurrence at 3 years of age. Clinical examination revealed an extensive molluscum contagiosum infection with more than 50 skin lesions. Immunological tests highlighted slightly decreased immunoglobulin levels and absence of vaccine immunization despite receiving vaccine boosts. T, B and NK cell counts were normal. Lymphocyte proliferation was normal in response to mitogens, impaired in response to tetanus toxoid, and abolished in response to varicella-zoster virus antigens. WES revealed an X-linked hemizygous insertion in exon 6 of *MAGT1* (NM_032121.5:c.786_787insCATAC; p.Thr263HisfsTer11, Fig. 1A) transmitted by the mother.

He is currently healthy under immunoglobulin replacement, growth hormone therapy and hydrocortisone supplementation.

The Combined Annotation Dependent Depletion (CADD), which is a tool for scoring the deleteriousness of single nucleotide variants, has a high score for both variants: 38 for the p.Arg331Ter and 33 for the p.Thr263HisfsTer11, suggesting nonsense-mediated decay. The p.Arg331Ter variant is classified as pathogenic in Clinvar (VCV000625837.3) and has been reported in another unrelated XMEN patient.[4] Moreover, serum transferrin analysis of both patients indicated an abnormal glycosylation pattern (Fig. 4A) with an increase in the disialylated glycoform. This suggested the presence of unoccupied N-glycosylation sites.

Thus, considering all clinical features, the predicted pathogenicity of *MAGT1* variants and the biochemical abnormalities, these patients were diagnosed with MAGT1-CDG.

XMEN patients display impaired platelet function

Platelet expression of MAGT1, which is of 2050 copies,[17] was undetectable in P1 and P2 (Fig. 1B). Absence of MAGT1 from fibroblasts and lymphocytes has previously been described in patients carrying other *MAGT1* mutations,[4] characterized as LOF variants. Analysis of hematological parameters showed normal platelet count and normal expression of key platelet receptors such as integrin $\alpha_{IIb}\beta_3$, GPIbα, GPIX, or GPVI (not shown). Platelet ultrastructure analysis demonstrated

abnormal elongated shapes in patient samples, in contrast to the discoid shaped ones of healthy donors (HDs). The unusual barbell-shaped proplatelets observed (8.2% and 8.8% for P1 and P2, respectively, *versus* 1.4% in HDs) suggested the presence of immature platelets (Fig. 1C),[18] indicating a role of MAGT1 in proplatelet maturation (further studies required). These unusual morphologies and MAGT1 expression were corrected after HSCT in P1 (Fig. 1B,C).

We next investigated the impact of the LOF of MAGT1 on platelet function in both patients. Platelet aggregation induced by low thrombin doses was impaired, but partially restored at higher concentrations (Fig. 1D). Strikingly, platelet aggregation in response to PAR1-AP was absent at low and high concentrations, and impaired at low doses of PAR4-AP (Fig. 1D). This indicated that the defects in thrombin-induced platelet aggregation were mostly dependent on PAR1 receptor. Platelet aggregation induced by collagen and ADP was also impaired (Fig. 1D). After HSCT, P1 exhibited normal aggregation profiles with all agonists tested (Fig. 1E), demonstrating that the observed defects were specifically related to MAGT1 deficiency in platelets.

To go further, activation of integrin $\alpha_{IIb}\beta_3$, a key receptor involved in platelet aggregation, was evaluated by flow cytometry (Fig. 2A). Both patients exhibited a severe deficit in integrin activation with thrombin, even at higher concentrations (56% and 71% decreases for P1 and P2 compared to HDs, respectively). Similar results were observed with convulxin and ADP. All defects were corrected in P1 after HSCT.

Integrin activation and subsequent PAR-dependent platelet aggregation, require the involvement of signaling pathways such as calcium signaling[19] and PKC activity.[20] The rapid and transient Ca^{2+} mobilization observed in HD was almost abolished in patients at low thrombin concentrations, partially impaired at higher concentrations, and corrected in P1 after HSCT (Fig. 2B). This impaired Ca^{2+} signaling could be due to a defective PAR1, to impaired magnesium homeostasis[1] and/or to functional defects in calcium channels due to abnormal N-glycosylation.[21,22] Furthermore, PKC activity was defective in P1 platelets with thrombin and PAR4-AP. No PKC activity was detected after PAR1-AP stimulation (Fig. 2C).

Due to the severe PAR1-dependent defects, PAR1 expression was investigated by western-blotting (Fig. 2D). While fully glycosylated PAR1 was detected between ~65 and ~85 kDa in HD platelets,[23] only smeared bands were observed between ~50 and ~60 kDa in P1 and P2. This result suggested a partial glycosylation defect of the receptor in patients, as incubation of platelet lysates with PNGaseF (removes all N-linked oligosaccharides from glycoproteins), eliminated the smeared bands. This partial deglycosylation could explain the PAR1-dependent defects. Indeed, it has been shown that N-glycosylation of PAR1 influences ligand docking and its signaling pathways.[24] Unfortunately, we were not able to identify fully deglycosylated PAR1. Therefore we cannot conclude whether PAR1-dependent defects were only due to the deglycosylation of PAR1, or whether they were also associated with impaired PAR1 expression.

Altogether, these results underline the severe impact of *MAGT1* mutations on PAR1-dependent platelet function, likely due to N-glycosylation defects.

Impaired platelet function in XMEN patients is associated with defective N-linked glycosylation

To further elucidate how MAGT1 deficiency could impact platelet function, we focused our investigations on defective N-linked glycosylation reported in XMEN disease.[4] We concentrated on several main platelet receptors. Integrin α_{IIb}, GPVI and GPIbα were fully glycosylated in HD samples however had lower molecular weights (MW) in XMEN samples, likely corresponding to underglycosylation (Fig. 3). To demonstrate that this decrease in MW was due to partial glycosylation of the receptors, platelet lysates were incubated with PNGaseF. A marked MW decrease of integrin α_{IIb} and GPVI by 14 kDa and 5.5 kDa, respectively, in HDs and patient samples was observed after PNGaseF treatment (Fig. 3A, B). The corresponding N-deglycosylated integrin α_{IIb} and GPVI showed no significant difference in MW between HDs and patients. These observations confirmed that the decreased MW of integrin α_{IIb} and GPVI in untreated platelets of P1 and P2 were due to a partial decrease of N-glycosylation on both receptors. Interestingly, the MW decrease did not affect all receptors in the same way; integrin β_3 and β_1 seemed normal (Fig. 3C,D) although 3 and 12 sites of N-glycosylation are predicted by NetNGlyc-1.0 server, respectively.[25] For GPIbα (Fig. 3E), a significantly lower MW band ($p<0.001$) was observed in both patients after PNGaseF treatment (130kDa) compared to HD (140kDa). This MW difference could not be attributed to an absence of sialic acid content on GPIbα, since α2-3 neuraminidase treatment did not affect it (not shown). We hypothesized that this could be due to a defect in plethoric O-glycans on GPIbα.[26] Indeed, defective N-linked glycosylation of enzymes/proteins important for O-linked glycosylation of GPIbα could cause this MW shift. This was also suggested for the defect observed in XMEN on apolipoprotein-CIII, which carries an O-glycosylation site.[6] Unfortunately, we were not able to confirm this hypothesis as O-glycosidase treatment of patient platelets prevented any correct detection of proteins by western blotting. Finally, in P1, all receptors analyzed recovered normal MW after HSCT, indicating an intrinsic role of MAGT1 in platelets.

Altogether, these data demonstrate a partial N-linked glycosylation defect on glycoproteins in platelets as previously described for the NKG2D receptor in T lymphocytes.[6]

To further characterize the XMEN-associated glycosylation defects, we analyzed N-glycosylation of liver-derived serum transferrin, and total serum and platelet N-glycomes from patients. Transferrin N-glycosylation patterns in patients showed a decrease in the major tetrasialylated glycoform compared to HDs, and a distinctive increase in the disialylated glycoform (Fig. 4A). N-glycoprotein macroheterogeneity arises from variations in N-glycosylation site occupancy, while microheterogeneity concerns the variations of N-glycan structures at a specific N-glycosylation site. Macroheterogeneity is caused by inefficient transfer of N-glycans to proteins, which is determined by the presence and function of OST subunits. Similar to how the OST complex is impacted in Signal Sequence Receptor Subunit 4 (SSR4)-CDG,[27] this result suggests the loss of one of two N-glycan chains of transferrin, therefore a partial under-occupancy of its glycosylation sites (macroheterogeneity). However total

serum and platelet N-glycan profiles of the patients proved overall similar to HD regarding N-glycan structures and corresponding relative abundancies, demonstrating absence of microheterogeneity (Fig. 4B,C). Therefore, these results consistently underline that XMEN patients can present partial (in the liver) or total (in platelets) defective N-glycosylation macroheterogeneity (for some proteins), without impacting N-glycan microheterogeneity. Hence, we hypothesize that the decreased MW of platelet receptors (Fig. 3) could be due to a partial defect of N-glycosylation site occupancy without modifications to the N-glycan structures.

In conclusion, we described here for the first time in two unrelated XMEN patients that MAGT1 deficiency has significant negative impacts on platelet function, causing severe thrombopathy, possibly by altering N-glycosylation in several platelet proteins.

ACKNOWLEDGMENTS

We are grateful to patients and their families for their cooperation in the study. We thank the CIQLE Centre d'Imagerie Quantitative Lyon-Est (France) for expert technical assistance with the electron microscopy studies and CEDI (Centre d'Etude des Déficits Immunitaires; Hôpital Necker-Enfants Malades, Paris, France) for biological investigations. This work was supported by INSERM.

AUTHOR CONTRIBUTIONS

AK, JS, MF, TV, CR, JCB, AB, FF, SC, DL, SK, AZ, FA designed, performed experiments, collected and analyzed the data; AK, CR, CM, FA wrote the manuscript; DB, CD, GMC, SL, EM critically reviewed the manuscript; CM, MT, BF, IP provided patient and family care, and monitored the patients.

CONFLICT OF INTEREST

The authors declare no conflict of interest.

REFERENCES

1. Li FY, Chaigne-Delalande B, Kanellopoulou C, et al. Second messenger role for Mg2+ revealed by human T-cell immunodeficiency. *Nature*. 2011;475(7357):471-476.

2. Chaigne-Delalande B, Li FY, O'Connor GM, et al. Mg2+ regulates cytotoxic functions of NK and CD8 T cells in chronic EBV infection through NKG2D. *Science*. 2013;341(6142):186-191.

3. Li FY, Chaigne-Delalande B, Su H, Uzel G, Matthews H, Lenardo MJ. XMEN disease: a new primary immunodeficiency affecting Mg2+ regulation of immunity against Epstein-Barr virus. *Blood*. 2014;123(14):2148-2152.

4. Blommaert E, Peanne R, Cherepanova NA, et al. Mutations in MAGT1 lead to a glycosylation disorder with a variable phenotype. *Proceedings of the National Academy of Sciences of the United States of America*. 2019;116(20):9865-9870.

5. Dimitrova D, Rose JJ, Uzel G, et al. Successful Bone Marrow Transplantation for XMEN: Hemorrhagic Risk Uncovered. *Journal of clinical immunology*. 2019;39(1):1-3.

6. Ravell JC, Matsuda-Lennikov M, Chauvin SD, et al. Defective glycosylation and multisystem abnormalities characterize the primary immunodeficiency XMEN disease. *The Journal of clinical investigation*. 2020;130(1):507-522.

7. Mammadova-Bach E, Jaeken J, Gudermann T, Braun A. Platelets and Defective N-Glycosylation. *International journal of molecular sciences*. 2020;21(16).

8. Adam F, Verbeuren TJ, Fauchere JL, Guillin MC, Jandrot-Perrus M. Thrombin-induced platelet PAR4 activation: role of glycoprotein Ib and ADP. *Journal of thrombosis and haemostasis : JTH*. 2003;1(4):798-804.

9. Berrou E, Soukaseum C, Favier R, et al. A mutation of the human EPHB2 gene leads to a major platelet functional defect. *Blood*. 2018;132(19):2067-2077.

10. Nurden P, Chretien F, Poujol C, Winckler J, Borel-Derlon A, Nurden A. Platelet ultrastructural abnormalities in three patients with type 2B von Willebrand disease. *British journal of haematology*. 2000;110(3):704-714.

11. Adam F, Kauskot A, Nurden P, et al. Platelet JNK1 is involved in secretion and thrombus formation. *Blood*. 2010;115(20):4083-4092.

12. Jeppsson JO, Arndt T, Schellenberg F, et al. Toward standardization of carbohydrate-deficient transferrin (CDT) measurements: I. Analyte definition and proposal of a candidate reference method. *Clinical chemistry and laboratory medicine*. 2007;45(4):558-562.

13. Parente F, Ah Mew N, Jaeken J, Gilfix BM. A new capillary zone electrophoresis method for the screening of congenital disorders of glycosylation (CDG). *Clinica chimica acta; international journal of clinical chemistry*. 2010;411(1-2):64-66.

14. Bruneel A, Cholet S, Drouin-Garraud V, et al. Complementarity of electrophoretic, mass spectrometric, and gene sequencing techniques for the diagnosis and characterization of congenital disorders of glycosylation. *Electrophoresis*. 2018;39(24):3123-3132.

15. Goyallon A, Cholet S, Chapelle M, Junot C, Fenaille F. Evaluation of a combined glycomics and glycoproteomics approach for studying the major glycoproteins present in biofluids: Application to cerebrospinal fluid. *Rapid communications in mass spectrometry : RCM*. 2015;29(6):461-473.

16. Ceroni A, Maass K, Geyer H, Geyer R, Dell A, Haslam SM. GlycoWorkbench: a tool for the computer-assisted annotation of mass spectra of glycans. *Journal of proteome research*. 2008;7(4):1650-1659.

17. Huang J, Swieringa F, Solari FA, et al. Assessment of a complete and classified platelet proteome from genome-wide transcripts of human platelets and megakaryocytes covering platelet functions. *Scientific reports*. 2021;11(1):12358.

18. Kemble S, Dalby A, Lowe GC, et al. Analysis of preplatelets and their barbell platelet derivatives by imaging flow cytometry. *Blood advances*. 2022;6(9):2932-2946.

19. Varga-Szabo D, Braun A, Nieswandt B. Calcium signaling in platelets. *Journal of thrombosis and haemostasis : JTH*. 2009;7(7):1057-1066.

20. Harper MT, Poole AW. Diverse functions of protein kinase C isoforms in platelet activation and thrombus formation. *Journal of thrombosis and haemostasis : JTH*. 2010;8(3):454-462.

21. Choi YJ, Zhao Y, Bhattacharya M, Stathopulos PB. Structural perturbations induced by Asn131 and Asn171 glycosylation converge within the EFSAM core and enhance stromal interaction molecule-1 mediated store operated calcium entry. *Biochimica et biophysica acta Molecular cell research*. 2017;1864(6):1054-1063.

22. Dietrich A, Mederos y Schnitzler M, Emmel J, Kalwa H, Hofmann T, Gudermann T. N-linked protein glycosylation is a major determinant for basal TRPC3 and TRPC6 channel activity. *The Journal of biological chemistry*. 2003;278(48):47842-47852.

23. Vouret-Craviari V, Grall D, Chambard JC, Rasmussen UB, Pouyssegur J, Van Obberghen-Schilling E. Post-translational and activation-dependent modifications of the G protein-coupled thrombin receptor. *The Journal of biological chemistry*. 1995;270(14):8367-8372.

24. Soto AG, Trejo J. N-linked glycosylation of protease-activated receptor-1 second extracellular loop: a critical determinant for ligand-induced receptor activation and internalization. *The Journal of biological chemistry*. 2010;285(24):18781-18793.

25. Gupta R, Brunak S. Prediction of glycosylation across the human proteome and the correlation to protein function. *Pacific Symposium on Biocomputing Pacific Symposium on Biocomputing*. 2002:310-322.

26. Li Y, Fu J, Ling Y, et al. Sialylation on O-glycans protects platelets from clearance by liver Kupffer cells. *Proceedings of the National Academy of Sciences of the United States of America*. 2017;114(31):8360-8365.

27. Castiglioni C, Feillet F, Barnerias C, et al. Expanding the phenotype of X-linked SSR4-CDG: Connective tissue implications. *Human mutation*. 2021;42(2):142-149.

28. Feng M, Elaib Z, Borgel D, et al. NAADP/SERCA3-Dependent Ca(2+) Stores Pathway Specifically Controls Early Autocrine ADP Secretion Potentiating Platelet Activation. *Circulation research*. 2020;127(7):e166-e183.

29. Watanabe Y, Aoki-Kinoshita KF, Ishihama Y, Okuda S. GlycoPOST realizes FAIR principles for glycomics mass spectrometry data. *Nucleic acids research*. 2021;49(D1):D1523-D1528.

FIGURE LEGENDS

Figure 1. Severe platelet dysfunction due to MAGT1 deficiency in XMEN disease

(**A**) Schematic representation of MAGT1 protein and localization of the two mutations carried by XMEN patients (P1 and P2). MAGT1 consists of a signal peptide (SP), a thioredoxin domain and four transmembrane (TM) regions.

(**B**) MAGT1 expression was evaluated in platelets of healthy donors (HDs) or XMEN patients by western-blotting. For P1, MAGT1 expression was also assessed after HSCT. Washed platelets ($3x10^8$/mL) were lysed in Laemmli sample buffer and reduced with 25 mM dithiothreitol (DTT). Platelet lysates (corresponding to $5x10^6$ platelets) were loaded onto the gel, separated by electrophoresis using a NuPage™ 4-12% Bis-Tris Protein gel (Invitrogen), then transferred to nitrocellulose membrane. Membranes were incubated overnight with the primary antibodies rabbit anti-MAGT1 (0.2 µg/mL; Proteintech) or mouse anti-β-actin (1/10000, used as loading control; R&D Systems), then with the secondary horseradish peroxidase (HRP)-coupled antibodies (Interchim): donkey anti-mouse IgG-HRP (1/10000, Interchim) or donkey anti-rabbit IgG-HRP (1/10000). Immunoreactive bands were visualized with enhanced chemiluminescence detection reagents (ECL) using a G:BOX Chemi XT16 Image System, then quantified using Gene Tools version 4.03.05.0 (Syngene). Representative blot (left panel) and mean ± SEM of MAGT1 expression (right graph) normalized to β-actin (HD is set to 1) from several independent experiments (HDs, *n* = 9; P1, *n* = 3; P1 after HSCT, *n* = 5; P2, *n* = 3) are presented. Statistical difference was evaluated by one-way ANOVA with Dunnett's post-test for multiple comparisons (*** p<0.001).

(**C**) Platelet ultrastructure was analyzed once for each patient using transmission electron microscopy (TEM). Platelet-rich plasma (PRP) was fixed by incubating for 1 hour at room temperature with 1.25% glutaraldehyde in 0.1 M phosphate buffer, pH 7.2, centrifuged for 10 minutes at 1100g, and washed once in phosphate buffer. Platelets were kept in 0.2% glutaraldehyde at 4°C until being processed by standard TEM for analysis of platelet morphology, as previously described.[9,10] Pictures represent two different magnifications (bottom higher magnification). Scale bar represents 1 µm. Graph shows the platelet morphology which is defined by the ratio between the large and the small diameter of the platelet. One hundred platelets were analyzed by TEM, and the graph represents the mean ± SEM. Statistical difference was evaluated by one-way ANOVA with Dunnett's post-test for multiple comparisons (* p<0.05).

(**D,E**) Aggregation of washed platelets (300 µL at 3.10^8/mL) induced by thrombin (80 and 150 mU/mL), PAR1-AP (10 and 100 µM), PAR4-AP (50 and 100 µM), collagen (1 and 2 µg/mL) or ADP (10 and 50 µM) was evaluated once for each patient (P1, P2 and P1 after HSCT) and HD.

Figure 2. Impairment of integrin $\alpha_{IIb}\beta_3$ activation, calcium signaling, PKC activity and glycosylated PAR1 due to MAGT1 deficiency in XMEN disease

(**A**) Integrin $\alpha_{IIb}\beta_3$ activation was evaluated once for each patient by flow cytometry (BD AccuriC6Plus), using a specific antibody, PAC1, which recognizes the active conformation of the integrin. Washed

platelets ($2x10^8$/mL) in Tyrode's buffer were stimulated or not for 10 minutes without stirring by a range of thrombin (100 to 1000 mU/mL), convulxin (75 to 600 pM; Pentapharm) or ADP (10 to 100 µM) concentrations. Platelet stimulation was then stopped by adding 1 mL Tyrode's buffer containing 2 mM $CaCl_2$, before incubation with fluorescein isothiocyanate (FITC) anti-human-activated $\alpha_{IIb}\beta_3$ integrin (clone PAC-1; Becton Dickinson; 20 µL of FITC-PAC1 for $5x10^5$ platelets) for 20 minutes at room temperature. Graphs represent the relative mean fluorescence intensity (MFI) of PAC1-binding to platelets of P1 (red; n=1), P2 (green; n=1) and P1 after HSCT (blue; n=1), compared to that of HD (black; n=3) platelets at the highest dose of thrombin (1000 mU/mL), convulxin (600 pM) or ADP (100 µM) that is set as 100%.

(**B**) Calcium mobilization was assessed once for HD (black), P1 (red), P2 (green) and P1 after HSCT (blue) by flow cytometry. Washed platelets ($3x10^8$/mL) were preincubated with the calcium fluorophore Oregon-green 488 BAPTA-1 AM (1 µM, Invitrogen) for 30 minutes à 37°C, then diluted at $3x10^6$/ mL in Tyrode's buffer. Calcium mobilization induced by thrombin (50 or 200 mU/mL) in absence of external Ca^{2+} (supplemented with EGTA 0.1 mM) was recorded in real time by flow cytometry as previously described.[28] The graphs represent Ca^{2+} mobilization defined as the ratio of MFI of activated *versus* resting platelets (set as 1) as a function of time in seconds. Arrow indicates the time of platelet stimulation by thrombin.

(**C**) PKC activity in HD and P1 platelets after stimulation for 3 minutes with a range of thrombin (90 to 500 mU/mL), PAR1-AP (10 to 100 µM) or PAR4-AP (75 to 100 µM) concentrations was indirectly analyzed once by assessing serine phosphorylation of PKC substrates by western-blotting. Washed platelets ($3x10^8$/mL) were lysed in Laemmli sample buffer and reduced with 25 mM DTT. Platelet lysates (corresponding to $5x10^6$ platelets) were loaded onto the gel, separated by electrophoresis using a NuPage™ 4-12% Bis-Tris Protein gel, then transferred to nitrocellulose membrane. Membranes were incubated overnight with the primary antibodies rabbit anti-Phospho-(Ser) PKC substrate (1/1000; Cell Signaling) or rabbit anti-14-3-3ζ (0.2 µg/mL; Santa Cruz), used as loading control for normalization, then with the secondary HRP-coupled antibody donkey anti-rabbit IgG-HRP (1/10000). The graphs show the phosphorylation index in arbitrary units (a.u.) obtained by the ratio between the signal intensity of a lane and that obtained without stimulation.

(**D**) PAR1 expression was evaluated in HD, P1, P2, P1 after HSCT (P1-H) and PNGase F-treated HD platelets by western-blotting. Platelet lysates ($5x10^6$ platelets) were reduced with 25 mM DTT and separated by electrophoresis using a NuPage™ 4-12% Bis-Tris Protein gel and transferred to nitrocellulose membrane. PAR1 protein was detected using mouse anti-PAR1 antibody (1 µg/mL; Clone ATAP2; Santa Cruz) and mouse anti-β-actin (1/10000) was used as loading control. In (C and D), dotted lines indicate that the samples were derived from the same gel but were non-contiguous. Arrow indicates a non-specific band because it was also found with mouse platelets (not shown), which do not express PAR1.

Figure 3. Restricted N-linked glycosylation of platelet glycoproteins

The molecular weights (MW) of (**A**) integrin α_{IIb}, (**B**) GPVI, (**C**) integrin β_3, (**D**) integrin β_1 and (**E**) GPIbα were evaluated in platelet lysates from healthy donors (HD), P1, P2 and P1 after HSCT (P1-H) by western-blotting before and after treatment with PNGase F. Washed platelets ($3x10^8$/mL) or PNGase F-treated platelets ($3x10^8$/mL) were lysed in Laemmli sample buffer and reduced with 25 mM DTT. Platelet lysates (corresponding to $5x10^6$ platelets) were loaded onto the gel, separated by electrophoresis using a NuPage™ 4-12% Bis-Tris Protein gel, then transferred to nitrocellulose membrane. Membranes were incubated overnight with the primary antibodies : mouse anti-CD41 (0.2 µg/mL, clone SZ22; Beckman Coulter), mouse anti-CD42b (GPIbα, 1 µg/mL, clone SZ2; Beckman Coulter), mouse anti-CD61 (0.05 µg/mL, clone 1; Beckman Coulter), rabbit anti-integrin β1 (0.2 µg/mL; Proteintech), or sheep anti-GPVI (0.2 µg/mL; R&D Systems), then with the secondary HRP-coupled antibodies: donkey anti-mouse IgG-HRP (1/10000), donkey anti-rabbit IgG-HRP (1/10000) or donkey anti-sheep IgG-HRP (1/5000). The graphs represent the mean MW variation ± SEM, (in kDa), for the patients compared to HDs, from at least 3 independent measures (for integrin α_{IIb} without treatment: HDs, n = 12; P1, n = 7; P1-HSCT, n = 4; P2, n = 5; for integrin α_{IIb} with PNGase F: HDs, n = 5; P1, n = 4; P1-HSCT, n = 3; P2, n = 4; for GPVI without treatment: HDs, n = 12; P1, n = 8; P1-HSCT, n = 9; P2, n = 8; for GPVI with PNGase F: HDs, n = 5; P1, n = 5; P1-HSCT, n = 9; P2, n = 8; for integrin β_3 without treatment: HDs, n = 11; P1, n = 6; P1-HSCT, n = 4; P2, n = 4; for integrin β_3 with PNGase F: HDs, n = 3; P1, n = 3; P1-HSCT, n = 3; P2, n = 3; for integrin β_1 without treatment: HDs, n = 9; P1, n = 7; P1-HSCT, n = 7; P2, n = 7; for integrin β_1 with PNGase F: HDs, n = 4; P1, n = 4; P1-HSCT, n = 4; P2, n = 4; for GPIbα without treatment: HDs, n = 17; P1, n = 11; P1-HSCT, n = 4; P2, n = 5; for GPIbα with PNGase F: HDs, n = 7; P1, n = 6; P1-HSCT, n = 4; P2, n = 4). In (**D**), arrows indicate mature integrin β_1 (#1) and N-deglycosylated integrin β_1 (#2). Statistical difference was evaluated by one-way ANOVA with Dunnett's post-test for multiple comparisons (*** $p< 0.001$).

Figure 4. N-glycosylation analysis of liver-derived serum transferrin and mass spectrometry-based profiling of serum and platelet N-glycans

(**A**) The capillary electrophoresis transferrin (Tf) profile was investigated for healthy donor (HD), P1, P1 after HSCT and P2. Briefly, Tf glycoforms were separated and further detected at 200 nm wavelength using the capillary electrophoresis CDT kit from Sebia (France), originally developed for alcohol abuse screening.[12,13] Tf glycoforms are separated based on their electrophoretic mobility, which depends on their charge and size. The number of negatively-charged terminal sialic acids affects charge, while the number and length of N-glycan chains affect the size. Using this kit in HDs, 4-sialo Tf corresponds to Tf bearing two complete biantennary, disialylated N-glycan chains; 5-sialo Tf corresponds to 4-sialo Tf bearing an additional sialylated antennae on one chain; 3-sialo Tf corresponds to 4-sialo Tf lacking one terminal sialic acid moiety; and 2-sialo Tf classically corresponds to the absence of one entire N-glycan chain (as depicted in the P1 profile). In patients, elevated 2-sialo Tf highlights the partial lack of one entire N-glycan chain in agreement with defects in the OST complex. Graphs represent, in y axis, the optical density and the migration time in arbitrary units (a.u.), in the x axis. The glycoform distributions

for HD, P1 before and after HSCT, and P2 are indicated in the table. Normal range values have been established internally after using CDT kit for several years.

(**B, C**) MALDI-TOF mass spectra of permethylated PNGase F-released N-glycans from (**B**) serum and (**C**) platelet samples. Measurements were performed in the positive-ion mode and all ions are present in sodiated [M+Na^+] form. Green circles, mannose; yellow circles, galactose; blue squares, N-acetyl glucosamine; red triangles, fucose ; purple diamonds, sialic acid. (*) polyhexose species. Briefly, serum samples (5 µL) and washed platelets ($5x10^6$) were diluted in 100 mM sodium phosphate buffer (pH 7.4) and 100 mM dithiothreitol solutions (final concentrations 20 mM and 10 mM, respectively, in a total volume of 49 µL) and glycoproteins were denatured by heating to 95°C for 5 min. Protein de-N-glycosylation consisted in incubating overnight at 37°C with 2U of PNGase F. After acidification, proteins were precipitated using ice-cold ethanol for 1 hour at -20°C. N-glycans released were purified using porous graphitic carbon solid phase extraction cartridges, and subsequently permethylated before another purification step using C18 spin-columns. MALDI-TOF mass spectra were obtained by accumulating 1000–5000 shots (depending on the samples) over the 500–5000 *m/z* range, and were further internally calibrated. Glycan calibrants used were [$Man_5HexNAc_2$ + Na^+] at *m/z* 1579.783, [$Gal_1Man_3HexNAc_2Fuc_1$ + Na^+] at *m/z* 2040.025, [$Sial_1Gal_2Man_3HexNAc_4$ + Na^+] at *m/z* 2431.209, [$Sial_2Gal_2Man_3HexNAc_4$ + Na^+] at *m/z* 2792.383, and [$Sial_3Gal_3Man_3HexNAc_5$ + Na^+] at *m/z* 3602.776. All glycomics data are available on https://glycopost.glycosmos.org[29] under the accession number GPST000333.

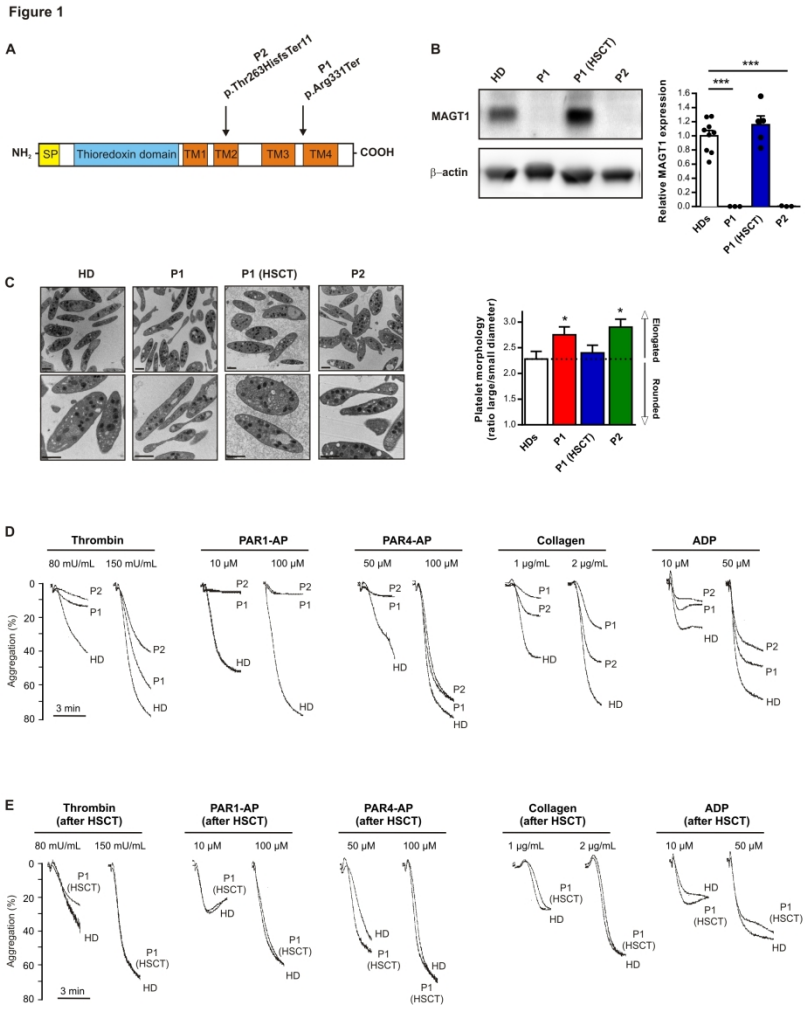

Figure 1

209x296mm (300 x 300 DPI)

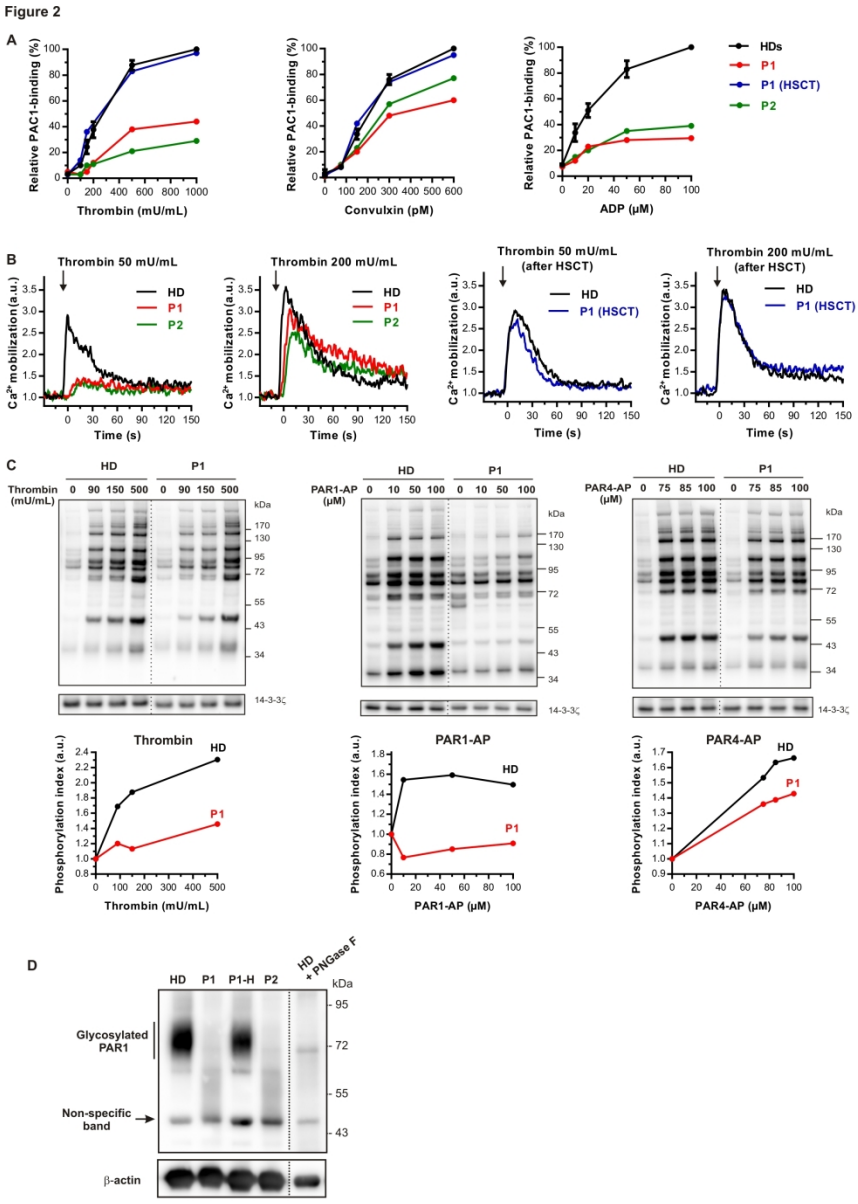

Figure 2

216x292mm (300 x 300 DPI)

Figure 3

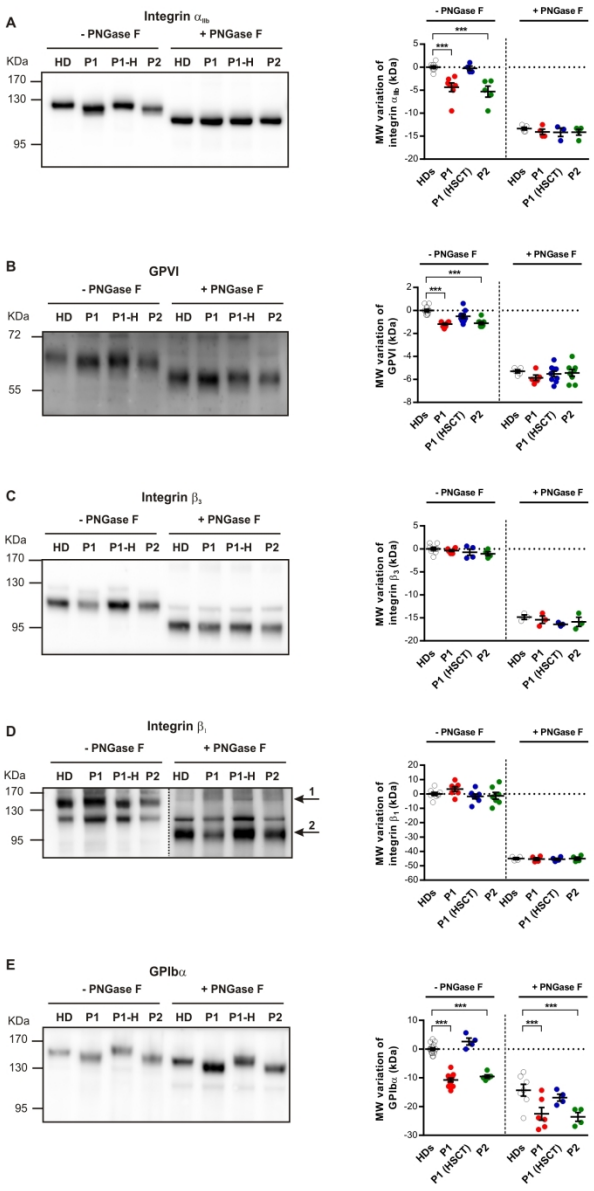

Figure 3

167x291mm (300 x 300 DPI)

Figure 4

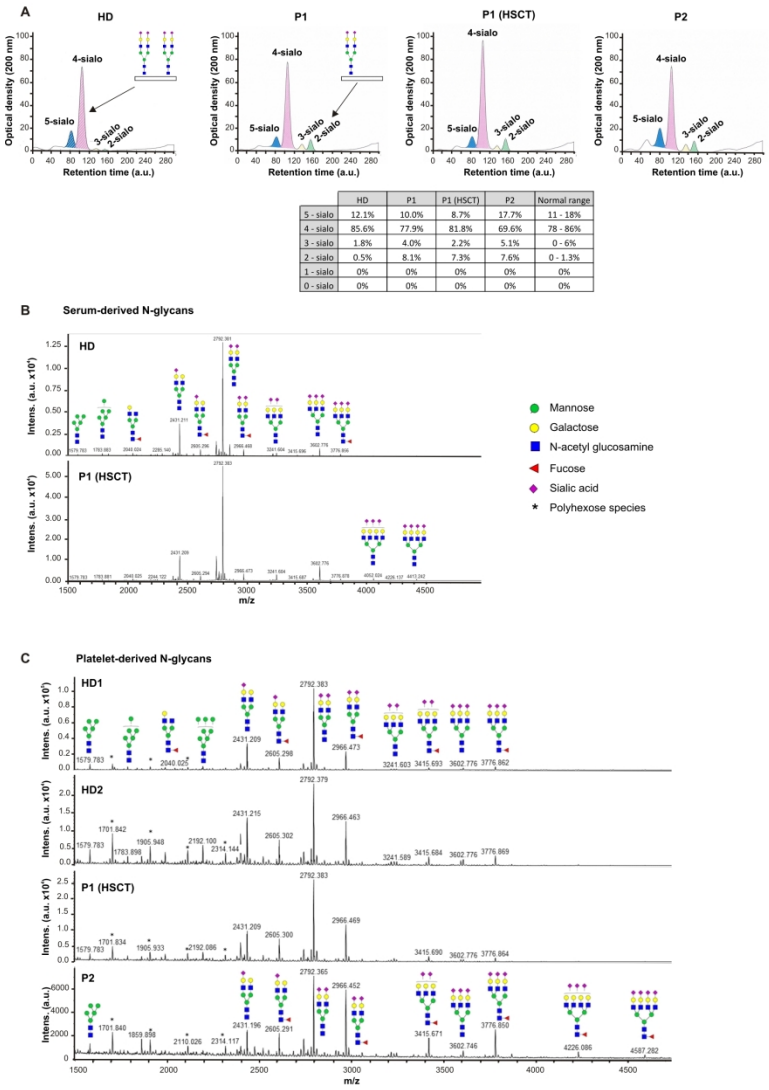

	HD	P1	P1 (HSCT)	P2	Normal range
5 - sialo	12.1%	10.0%	8.7%	17.7%	11 - 18%
4 - sialo	85.6%	77.9%	81.8%	69.6%	78 - 86%
3 - sialo	1.8%	4.0%	2.2%	5.1%	0 - 6%
2 - sialo	0.5%	8.1%	7.3%	7.6%	0 - 1.3%
1 - sialo	0%	0%	0%	0%	0%
0 - sialo	0%	0%	0%	0%	0%

Figure 4

205x311mm (300 x 300 DPI)